Journal of Cancer Research and Clinical Oncology (2025) 151:106
https://doi.org/10.1007/s00432-025-06150-9

RESEARCH

Chronic lymphocytic leukemia (CLL) screening and abnormality detection based on multi-layer fluorescence imaging signal enhancement and compensation

Lemin Shi[1,2] · Ping Gong[2] · Mingye Li[3,4] · Dianxin Song[2] · Hao Zhang[2] · Zhe Wang[2] · Xin Feng[1]

Received: 31 December 2024 / Accepted: 24 February 2025

Abstract

Purpose Fluorescence in situ hybridization (FISH) plays a critical role in cancer screening but faces challenges in signal clarity and manual intervention. This study aims to enhance FISH signal clarity, improve screening efficiency, and reduce false negatives through an automated image acquisition and signal enhancement framework.

Methods An automated workflow was developed, integrating a dynamic signal enhancement method that optimizes global and local features. An improved Cycle-GAN network was introduced, incorporating residual connections and layer-wise supervision to accurately model and compensate for complex signal characteristics. Key metrics such as signal brightness, edge gradients, contrast improvement index (CII), and structural similarity index (SSIM) were used to evaluate performance.

Results The proposed method increased weak signal brightness by 49.02%, edge gradients by 48.61%, and CII by 32.52%. The SSIM reached 0.996, indicating high fidelity to original signals.

Conclusion Visual analysis demonstrated clearer, more continuous, and uniform fluorescence signals, effectively mitigating fragmentation and uneven distribution. These improvements reduced false negatives and enhanced genomic abnormality detection accuracy. The proposed method significantly improves FISH signal clarity and stability, providing reliable support for cancer screening, genomic abnormality detection, molecular typing, prognosis evaluation, and targeted treatment planning.

Keyword Fluorescence in situ hybridization (FISH); feature enhancement; cyclic generative adversarial network (Cycle-GAN); cancer screening

Introduction

Fluorescence in situ hybridization (FISH) is a critical technique in subcellular biology, widely applied to investigate genomic spatial organization and gene expression. It has played a vital role in elucidating the genomic mechanisms of chronic lymphocytic leukemia (CLL) (Bloehdorn et al. 2021). By precisely detecting abnormalities in key genes such as RB1, DLEU, and LAMP, FISH has uncovered molecular insights, including the tumor suppressor function loss of RB1, microRNA dysregulation caused by DLEU, and the immune evasion potential associated with LAMP1. These findings have provided a foundation for molecular subtyping, prognosis evaluation, and targeted therapies for CLL patients, linking specific gene deletions to clinical outcomes and fostering therapeutic innovation.

Despite its importance, FISH technology faces limitations in detecting complex structural variations and small mutations, as well as challenges like signal attenuation and background noise interference, especially in the analysis of weak signals (Safaee et al. 2024; Trieu et al. 2019; Yang et al. 2025). Additionally, the labor-intensive and time-consuming workflows, along with reliance on manual analysis, make it difficult to scale for high-throughput applications.

✉ Xin Feng
fengxin@cust.edu.cn

1 School of Computer Science and Technology, Changchun University of Science and Technology, Changchun 130032, China

2 School of Life Science and Technology, Changchun University of Science and Technology, Changchun, Jilin 130032, China

3 Department of Information Systems and Business Analytics, RMIT University, Melbourne, VIC 3001, Australia

4 School of Computing and Information Systems, University of Melbourne, Parkville, VIC 3010, Australia

Published online: 11 March 2025

In recent years, deep learning has made significant strides in overcoming challenges in fluorescence imaging and genomic research. (Tian et al. 2023) enhanced image quality using deep learning; however, reliance on labeled datasets restricts its generalizability. Li. H et al. (2021a, b) improved low-light imaging quality, but the approach demands substantial computational resources. For RNA spot detection, (Eichenberger et al. 2021), developed a threshold-free method, whereas Bouilhol (2022) and Mabaso (2018) employed convolutional neural networks (CNNs) to enhance accuracy, However, these methods exhibit limited robustness in noisy environments. Similarly, Liu's HRDNet (Liu et al. 2021) improved resolution for small objects, but its high computational demands limit practical applications. Dheeraj Agrawal (2024) proposed an image enhancement algorithm that improves the visual effects and quantitative indicators of low-light or hazy images by fusing illumination estimation, dehazing filter and discrete wavelet transform. Simulation results show that this method outperforms traditional algorithms in visibility and performance.

Automated segmentation and 3D imaging facilitate genomic analysis. AC Yadav (2025) proposed an MRI-based brain tumor segmentation model based on the U-NET network, aiming to optimize image fidelity, including noise reduction and spatial alignment to ensure the highest quality input for the segmentation model, enhancing precision in detecting and delineating intricate brain tumor boundaries and advancing the effectiveness of medical image analysis. Memmel's FocAn tool (Memmel et al. 2020) improved DNA repair focus analysis, but its applicability is limited. Lew (2021) emphasized the consistency of the automated pathology system. Wang's automated FISH signal analysis (Wang et al. 2012) simplified the workflow but relied on manual parameter adjustment, while Li's high-throughput tilt scanning (Li et al. 2021a, b) improving the speed and efficiency of whole-slide imaging in pathology, but pointed out the lack of flexibility.

Three-dimensional reconstruction of fluorescence in situ hybridization can help researchers observe and understand the spatial relationship of the genome in cells or tissues, reveal the three-dimensional structure and spatial arrangement of the genome, help understand the sequence, location and interaction of the genome, and conduct research on gene expression and regulatory mechanisms. Imbert (2022) A highly modular software was launched that can be used to segment nuclei and cells, detect and quantify RNA, and visualize results at the single-cell level. However, there are performance bottlenecks when processing large-scale 3D data, and the user interface still needs to be optimized. Frankenstein's Confocal scanning (Stachelek et al. 2022) 3D scoring tool (Frankenstein et al. 2021) improved FISH image analysis efficiency, though rare spot detection remained problematic. Wang (2023a, b) the application of Hi-C technology in disease mechanism research was discussed, and its difficulties in noise processing and the association between Hi-C maps and functional analysis were pointed out. Abdelhedi (2019) linked DPY19L2 defects to chromatin abnormalities, Revealing abnormalities in chromatin organization. Kloetgen (2020) studied the dynamic changes of chromosomes in acute leukemia and revealed the relationship between chromosome remodeling and disease occurrence, but the analysis efficiency was low and the functional research was insufficient. Kulasinghe (2020) used 3D-DNA FISH technology to detect ALK abnormalities in non-small cell lung cancer, but the sensitivity, specificity and data acquisition of this technology in clinical translation still need to be optimized.

This article proposes a series of solutions to the problem that weak signals in fluorescence microscope image acquisition are easily blurred or attenuated by defocus and optical characteristics, as well as inaccurate signal detection caused by background noise interference:

1. Automated image acquisition and processing:

An automated workflow for fluorescence microscopy was developed, enabling real-time image sharpness evaluation and automatic focal positioning. A high-quality dataset of in-focus, out-of-focus, and low-signal fluorescence images laid the foundation for a Cycle-GAN-based fluorescence signal compensation network.

2. Integrated feature analysis method:

A novel global–local feature analysis method dynamically computed global and local weights to suppress defocus-related background noise while enhancing weak signal resolution and saliency, improving signal visibility.

3. Cycle-GAN-based fluorescence signal compensation network:

Enhanced with residual connections and multi-layer convolution modules, the Cycle-GAN network adaptively optimized signal brightness and contrast through end-to-end training and hierarchical supervision, mitigating signal attenuation.

4. Visual analysis of signal compensation effects:

Comprehensive evaluations showed that the proposed method effectively resolved issues like signal breaks and uneven distribution, producing clearer, more coherent

fluorescence signals and improving the visibility of weak signal regions.

Materials and methods

Chronic lymphocytic leukemia (CLL) is characterized by slow progression, high clinical heterogeneity, and distinct genetic and epigenetic features, making it an ideal model for studying disease progression, personalized treatment, and cancer biomarkers. CLL samples typically exhibit weak and uneven fluorescence signals under fluorescence microscopy, along with high background noise and signal out-of-focus. Therefore, these samples are suitable for testing and validating methods for signal enhancement, denoising, and feature compensation to assess the applicability and stability of the proposed methods in clinical environments. Using XL RB1/DLEU/LAMP1 deletion probes and fluorescence in situ hybridization (FISH), three distinct loci in the 13q14 region of chromosome 13 in humans are targeted to investigate whether the pathogenesis of CLL is associated with fluorescence signal loss (Nelson et al. 2007) (Supplementary Information note 1).

Automated fluorescence microscope imaging process

In traditional image acquisition processes, operational errors and insufficient reproducibility often lead to inconsistent experimental results. Additionally, weak fluorescence signals are prone to blurring or even loss when out of focus, significantly degrading image quality. Manual adjustments of focus and image clarity assessment are also inefficient, failing to meet the demands for high-throughput and rapid processing. To address these issues, this paper proposes an automated imaging process for fluorescence microscopes, which includes four key steps: (1) Sample Positioning: The microscope moves to the target area without low-magnification scanning. (2) Focus Adjustment: The stage descends in 0.8 μm increments, capturing 150 images to determine the optimal focus using an energy gradient algorithm. (3) Image Acquisition: 11 images are taken at 0.44 μm intervals within a 2.2 μm z-stack range for each field of view. (4) Field Repetition: The process is repeated for all sample areas to ensure complete coverage. This automated process improves efficiency, reproducibility, and image quality, meeting high-throughput demands (Fig. 1 and Supplementary Information note 2).

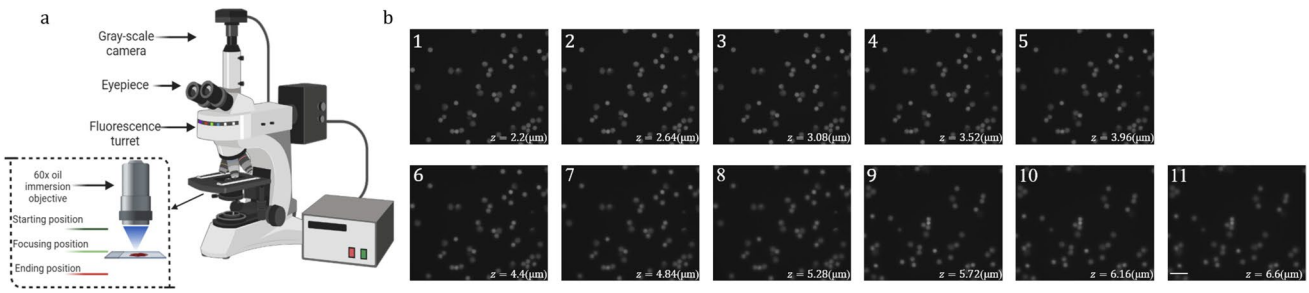

Fig. 1 Fluorescence microscope. **a** Image Acquisition. **b** Collection principle, Scale bar: 50 μm

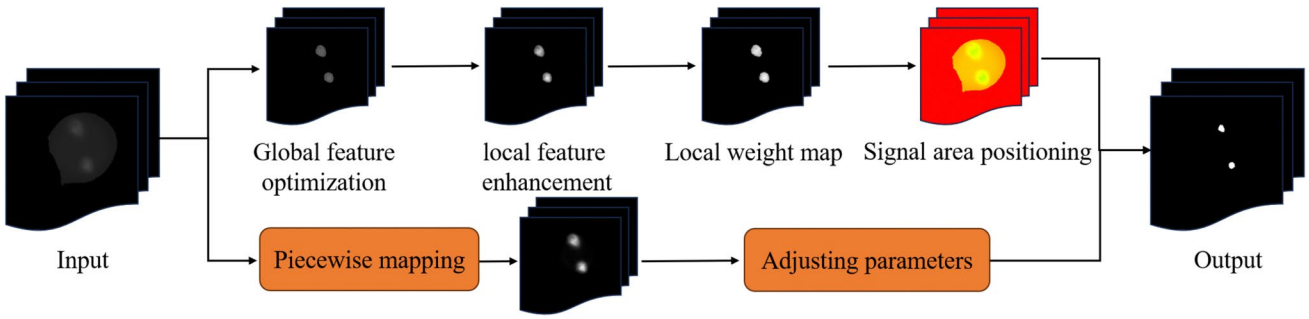

Fig. 2 Fluorescence Signal Enhancement Method

Fusion of regional and local feature analysis methods

To address common issues in fluorescence imaging, such as uneven brightness distribution, loss of detail, and background noise effect, this section proposes a region-weighted and local feature analysis method. The overall structure is shown in Fig. 2.the method begins by segmenting the nuclei from 11-layer(z-stack) fluorescence feature images, generating individual nuclear images (256×256 pixels). Global average and maximum values are dynamically calculated to generate weights, adjusting brightness distribution and achieving a naturally balanced visual effect. Spatial weight maps are generated using local feature maps and convolution, highlighting key areas while suppressing background noise. by combining 16-neighborhood averaging to fine-tune the brightness range, the method compensates for dark areas, midtones, and highlights separately, balancing overall brightness and enhancing local details.

(1) Global dynamic feature optimization

The purpose of global feature optimization is to enhance the overall brightness characteristics of grayscale images, making them more balanced and suitable for subsequent processing. The specific method involves calculating the global average and maximum brightness of the entire image using the following formulas:

$$\mu_c = \frac{1}{|\Omega|}\int X_c(x,y)dxdy \tag{1}$$

$$Max_c = \sup\{X_c(x,y)|(x,y)\in\Omega\} \tag{2}$$

Here, $|\Omega|$ represents the total number of pixels in the image. The pixel grayscale value at $X_c(x,y)$ in a continuous grayscale distribution scenario is calculated, where u_C is the global average value, and sup denotes the least upper bound of the pixel grayscale values, i.e., the global maximum value Max_C.

The average value μ_c reflects the overall brightness trend, while the maximum value Max_c represents the brightest part of the brightness range. A dynamic adjustment coefficient W_c is generated for the entire image, which is used to control image enhancement, compression, or brightness range mapping. This ensures the visual effect of the image appears more natural.

$$W_c = (\alpha \bullet \mu_c + \beta \bullet Max_c + \gamma) \tag{3}$$

A representative set of image datasets was selected for analysis, and under each parameter setting, both subjective perceptions and objective indicators (such as image sharpness and signal-to-noise ratio) were calculated for the enhanced images. Through multiple experiments, the parameters α (brightness adjustment), β (contrast enhancement), and γ (detail enhancement) were adjusted to optimize the enhancement effect of the fluorescence image. Professional doctors were invited to subjectively score the fluorescence images under each parameter combination. After multiple experiments and data analysis, the results showed that when $\alpha=0.6$, $\beta=0.4$, and $\gamma=0.1$, the enhanced image was closest to the real visual effect in terms of fluorescence characteristics. At this time, the image reached a relatively balanced state in terms of brightness, contrast, and detail expression, which not only retained sufficient image details but also avoided distortion that may be caused by excessive enhancement. the generated W_c was ultimately compressed to the range [0,1] for adjusting image brightness or contrast.

After dynamic weight adjustments, the pixel values ensured balanced overall image brightness, making the images more suitable for visual observation or subsequent processing.

$$X_c'(x,y) = W_c \bullet X_c(x,y) \tag{4}$$

(2) Local dynamic feature enhancement

The purpose of local feature optimization is to highlight prominent local regions in the image (such as edges and high-brightness areas) while suppressing the background or less significant regions.

$$\mu(i,j) = \frac{1}{|N(i,j)|}\int X_c(x,y)dxdy \tag{5}$$

$$Max(i,j) = \sup\{X_c(x,y)|(x,y)\in N(i,j)\} \tag{6}$$

For each value at position (i,j), the local mean $\mu(i,j)$ and local maximum $Max(i,j)$ are calculated.

In this process, $N(i,j)$ represents a local (3×3) neighborhood window centered on the pixel (i,j). The mean and maximum values from this neighborhood are extracted and concatenated to form a feature map. This feature map, denoted as $F(i,j)$, is then processed through a convolution operation:

$$X_c'' = (Conv(F(i,j))) \bullet X_c' \tag{7}$$

Conv represents the convolution kernel function, which is responsible for generating the spatial weight map. This operation ensures a smoother weight distribution across the feature map. By utilizing the local weight map, the weights of individual pixels are adaptively adjusted to emphasize prominent regions and enhance local details. This refinement ultimately leads to the generation of the final output feature map, preserving crucial information while improving spatial consistency.

(3) Segmented signal region optimization

The local maximum $L_{max}(i,j)$ and local minimum $L_{mix}(i,j)$ represent the least upper bound and greatest lower bound of grayscale values, respectively, within the 3×3 neighborhood window centered at (x,y).

$$L_{max}(x,y) = \sup\{I(x,y)|(x,y) \in N(i,j)\} \tag{8}$$

$$L_{mix}(x,y) = \inf\{I(x,y)|(x,y) \in N(i,j)\} \tag{9}$$

The local minimum R_1 is defined as the greatest lower bound (infimum) of the local minimum values, the local maximum R_2 is described as the least upper bound (supremum) of the local maximum values:

$$R_1 = \inf\{L_{mix}(i,j)|(i,j) \in \Omega\} \tag{10}$$

$$R_2 = \sup\{L_{max}(i,j)|(i,j) \in \Omega\} \tag{11}$$

By using a heatmap, high-intensity signal regions in the image (prominent fluorescence signal areas) can be quickly located. The neighborhood average value around the maximum fluorescence signal edge (4×4) is calculated, enabling a more precise analysis of the local environment of fluorescence characteristics. Based on this, the parameters of the piecewise linear function can be adjusted accordingly.

$$avg(p) = \frac{1}{|N_{16(P)}|}\int I(x,y)dxdy \tag{12}$$

Let $N_{16(P)}$ represent the 16-neighborhood centered at pixel p, and $avg(p)$ denote the average pixel value within this neighborhood.

(4) Dynamic optimization of piecewise linear enhancement

Based on the neighborhood average value range of different images $I(x,y)$, three piecewise intervals are defined: R_1:the local minimum grayscale value of the image. R_2 the local maximum grayscale value of the image.

According to the value range of $avg(p)$, the corresponding enhancement slopes (Zhang et al. 2023) $k_1 = S1/R2, k_2 = (S2-S1)/(R2-R1), k_3 = (250-s2)/(250-r2)$ are selected to enhance the image dynamically. all current gray values higher than R2 are mapped to a gray value of 255 in the output image (S2 = 255), so we compress the gray value of the original image (R1 is 0), remove the background noise other than the fluorescent features, and then amplify the gray value between (R1 = R2), and the gray value between R1 and R2 is linearly mapped.

$$O(x,y) = \begin{Bmatrix} k_1 \bullet I(x,y) & if avg(p) < R_1 \\ k_2 \bullet \left(I(x,y) - R_1\right) + S_1 & if R_1 \le avg(p) < R_2 \\ k_3 \bullet \left(I(x,y) - R_2\right) + S_2 & if avg(p) \ge R_2 \end{Bmatrix} \tag{13}$$

Here: k_1 is used to enhance the brightness of signal regions. k_2 ensures a smooth transition in medium-brightness areas, enhancing gradient details in the signal. k_3 suppresses overly bright regions while preserving details in high dynamic range areas.

After piecewise linear transformation, the final compensated image is generated.

$$R(x,y) = O(x,y) \bullet X_c'' \tag{14}$$

Fluorescence signal compensation network based on cycle-GAN

In order to better compensate for the intensity of the fluorescence signal, Zhu (Goodfellow et al. 2014; Zhu et al. 2017) introduced the Cycle-Consistency Generative Adversarial Network (Cycle-GAN), which performs image translation on unpaired data using a generator and a discriminator. Cycle-GAN employs cycle-consistency loss to ensure that the generated image remains consistent with the original during inverse transformations, thereby preserving fluorescence features. Its independence from paired data, strong detail retention, and flexibility make it a promising solution for enhancing insufficient fluorescence signals.

However, Cycle-GAN has certain limitations, including long training times, limited compensation capability in extremely weak signal regions, and insufficient optimization of fine-grained features. this study optimizes Cycle-GAN by introducing the following enhancements: Preprocessing with Multi-layer Fluorescence Image Feature Fusion and Precise Segmentation: To improve signal intensity characteristics using both regional and local feature analysis. Combination of Unsupervised and Supervised Learning: Incorporates a layer-wise supervision mechanism in the generator, utilizing limited real paired data to optimize generation results. transformer Module in the Generator: Designed with residual blocks to retain fine details and enhance feature extraction capabilities. Enhanced Discriminator: Adds multi-layer convolution operations and a fully convolutional classification layer to improve the discrimination of fluorescence features. Multiple Loss Constraints: Includes generation loss, cycle-consistency loss, and adversarial loss, ensuring greater realism and consistency when generating compensated images. The overall net-work structure is shown in Fig. 3.

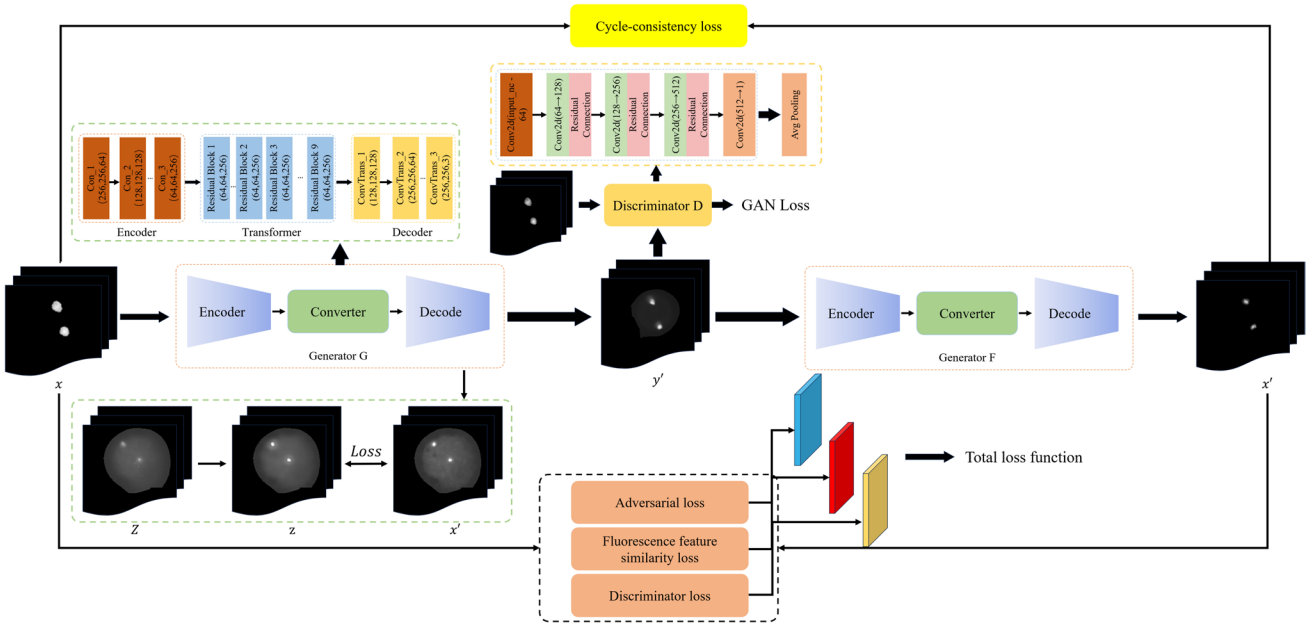

Fig. 3 Overall Network Structure

1. Hybrid unsupervised-supervised learning framework

Integrates a layer-wise supervision mechanism within the generator, effectively utilizing a limited set of real paired data to guide and refine the generation of fluorescence-enhanced images. The training process uses the Adam optimizer, which dynamically adjusts learning rates based on first and second moment estimates, ensuring faster convergence, improved training stability, and overall efficiency. By balancing unsupervised learning (for broader feature adaptation) with supervised refinement (for precise correction), the model enhances fidelity in fluorescence signal reconstruction.

2. Transformer-based feature enhancement in the generator

Incorporates residual blocks into the generator to preserve fine-grained image details and improve feature extraction, preventing the loss of important fluorescence information. This allows the generator to focus on critical fluorescence regions and improve spatial relationships between varying fluorescence intensities. Optimized using Adam, which dynamically refines parameter updates, ensuring stable feature learning while mitigating gradient vanishing and over-smoothing.

3. Enhanced discriminator:

Integrates multi-layer convolutional operations, enabling the model to progressively analyze fluorescence intensity variations across different scales, leading to more robust discrimination of signal artifacts and noise. This enhances the model's ability to distinguish fluorescence signal patterns while maintaining computational efficiency. The Adam optimizer is used to iteratively refine discrimination accuracy, adapting to complex fluorescence distributions and improving robustness against noise.

4. Multiple Loss Constraints:

Includes generation loss, cycle-consistency loss, and adversarial loss, ensuring enhanced realism, consistency, and accuracy in the generated compensated images.

The proposed optimizations significantly improve the compensation performance of Cycle-GAN, particularly in weak signal regions, while maintaining fine-grained feature details (Supplementary Information note 3 and Fig. 1).

To enhance fluorescence signal features, a multi-layer fluorescence image dataset is selected as the original image domain X. After regional local feature analysis, an enhanced fluorescence feature image x is generated, a sample library is constructed, and the image is trained end-to-end. *Lossfunction_X* measures the difference between the enhanced fluorescence image x and the fluorescence feature compensation image y' generated by the generator G.

Lcyc_X represents the difference between the enhanced image x and the converted image $x\prime$ generated by the generator F, and L_{GANXY} represents the distribution difference between the generated fluorescence feature compensation image $y\prime$ and the multi-layer fluorescence feature fusion image domain Y.

The generator G is trained to map $G : X \rightarrow Y$, ensuring that the generated sample $y = G(X)$ aligns as closely as possible with the distribution of the real fluorescence image domain Y. Meanwhile, the inverse mapping $F : Y \rightarrow X$ ensures that $x = G(y)$ maintains consistency with the distribution of the multilayer fluorescence feature image domain X.

Discriminators DX, DY are introduced to differentiate between real and generated fluorescence images. These discriminators evaluate whether the generated fluorescence feature images are real or synthetic. Through adversarial training between the generator and discriminators, the system gradually approaches a dynamic equilibrium point (Supplementary Information Fig. 2).

In the supervised learning phase, the model is further optimized with limited paired data. By applying z-stack supervision to the generator, utilizing a small number of real multilayer fused fluorescence images (see Supplementary Information Fig. 3), the model can more accurately capture fluorescence features. This enhances the realism and consistency of the generated images. The robust supervision process alleviates the challenges posed by the limited labeled data, significantly improving the model's ability to learn detailed fluorescence signals and thereby achieving the goal of generating compensated fluorescence images. A small set of feature images serves as dataset X, while real multilayer fused fluorescence feature images (Z) are used for step-by-step training of the generative network, as shown in (Supplementary Information note 4).

Results

Experimental environment

The fluorescence microscopy image dataset used in this study was independently collected and constructed by the authors to ensure its high relevance and applicability to the research objectives. The dataset consists of 800 fluorescence-labeled images, including focused images, defocused images, and low-light signal images. We used an Olympus BX61 upright fluorescence microscope, equipped with a 60 × oil objective lens (oil immersion objective lens), used with a 10 × eyepiece, with a total magnification of 600x, an objective numerical aperture of 1.4, a resolution of 2448 × 2048, and supports 11-layer (z-stack) image acquisition, which fully meets the needs of studying chromosome spatial distribution and genomic marker signal detection. According to the experimental requirements, the UV exposure time was set to 20 ms; for the three fluorescent dyes, the exposure time was optimized within the range of 200 ms to ensure the clarity of the signal and the sensitivity of the experiment, while effectively reducing the impact of photobleaching.

Training parameters were as follows:

Batch size was set to 1, considering the high-resolution nature of fluorescence images and memory constraints in Cycle-GAN training. Training was conducted for 200 epochs, ensuring sufficient optimization. Initial learning rate was set to 0.0005, and a linear decay strategy was applied, gradually reducing it to 0.0002 over the training process. The alpha value was set to 0.5 to balance the adversarial loss between the generator and discriminator, ensuring stable training dynamics. The dataset used for training consists of two parts, supporting both unsupervised and supervised learning: Unpaired Data: 600 unpaired multilayer fluorescence feature images, serving as the primary data source for unsupervised learning, enabling Cycle-GAN to learn feature transformations without direct supervision. Paired Data: 200 paired multilayer fluorescence feature images, used in supervised learning to optimize the generator layer by layer via pixel-wise reconstruction loss and feature similarity loss, improving realism and detail fidelity. These paired data are used for the supervised learning portion to optimize the generator layer by layer by directly calculating the differences (e.g., pixel-level loss or feature similarity loss) between the generated images and target images, thereby improving the realism and detail fidelity of the generated images.

Comparison of model performance

The performance of several models was compared, including GAN (Pan et al. 2023), VAE(Wang et al. 2022), traditional Cycle-GAN (Chen et al. 2024), and Pix2Pix (Kim et al. 2024) (baseline network). The proposed network demonstrates It achieves faster convergence, with significant loss reduction during the first 50 epochs, and stabilizes by 150 epochs, indicating high robustness and efficiency. Unlike GAN and Cycle-GAN, which exhibit significant early-stage loss fluctuations, and VAE, which struggles with fine detail retention, the proposed network effectively balances feature retention and compensation. By leveraging cycle consistency loss, fluorescence feature similarity loss, and adversarial loss, the network significantly enhances fluorescence signal intensity and detail, particularly after the fifth layer. These results highlight its capability to deliver stable and accurate

fluorescence signal compensation, making it a highly effective solution for complex imaging tasks (Supplementary Information note 5 and Fig. 4–5).

The loss curve of the strongly supervised network indicates continuous optimization, with the model progressively im-proving its fitting capability to the data (Supplementary Information Fig. 6.a). During the early training phase, the sharp decline in loss reflects the model's ability to quickly learn the main features of the data. In the later stages, the loss stabilizes, suggesting that the model is approaching a state of convergence with stable performance. the fluorescence feature compensation curve illustrates the performance of different methods in image feature compensation. Each curve represents a different method, with the vertical axis indicating the percentage of compensation effect and the horizontal axis corresponding to the image index.

It is observed that the proposed method shows a significant improvement in compensation effects after the fifth layer of images. This demonstrates the clear advantage of the proposed method in enhancing fluorescence features (Supplementary Information Fig. 6.b).

Evaluation of experimental results

To validate the effectiveness of the algorithm, both subjective visual evaluation and objective metric evaluation were employed. In the visual evaluation, the results of the proposed algorithm were directly compared with those of network compensation methods. By observing the images processed by different algorithms, the performance in enhancing details, improving clarity, and enhancing overall visual effects was assessed. Objective metrics were used to evaluate image quality, including Structural Similarity Index (SSIM) (Osorio et al. 2022), Contrast Improvement Index (CII) (Suradi and Abdullah 2021), Contrast (Wang et al. 2020), and Energy of Gradient (EOG) (X. Wang et al. 2023a, b). These metrics quantitatively measured the quality changes before and after image processing, including image clarity, contrast, and structural fidelity.

The enhancement algorithm operates selectively on each fluorescence channel, prioritizing the compensation of channels with low brightness or weak signals while maintaining stability and non- effect areas with no signal or saturated signals. This demonstrates the precision and selectivity of the enhancement process. The enhanced images exhibit improvements in brightness and contrast, particularly strengthening the fluorescence signal intensity in key layers(z-stack). Notably, the algorithm significantly enhances the brightness and detail clarity in regions with weak signals. The proposed network demonstrates superior performance in fluorescence signal compensation compared to traditional models. It achieves the highest SSIM (0.999), indicating near-perfect similarity to the original images, and shows significant improvements in contrast (49.02%) and edge gradient (EOG, 48.61%). The contrast improvement index (CII) ranges from 1.021 to 1.353, reflecting effective and balanced enhancement without over-compensation. According to the statistical analysis results provided, this method does show significant improvements compared with other methods (such as CycleGAN, Cycle, Pix2Pix) in multiple indicators. This method is significantly better than other methods in SSIM, Contrast and EOG, and shows significant improvements compared with CycleGAN, Cycle and Pix2Pix (all p values are less than 0.05). In

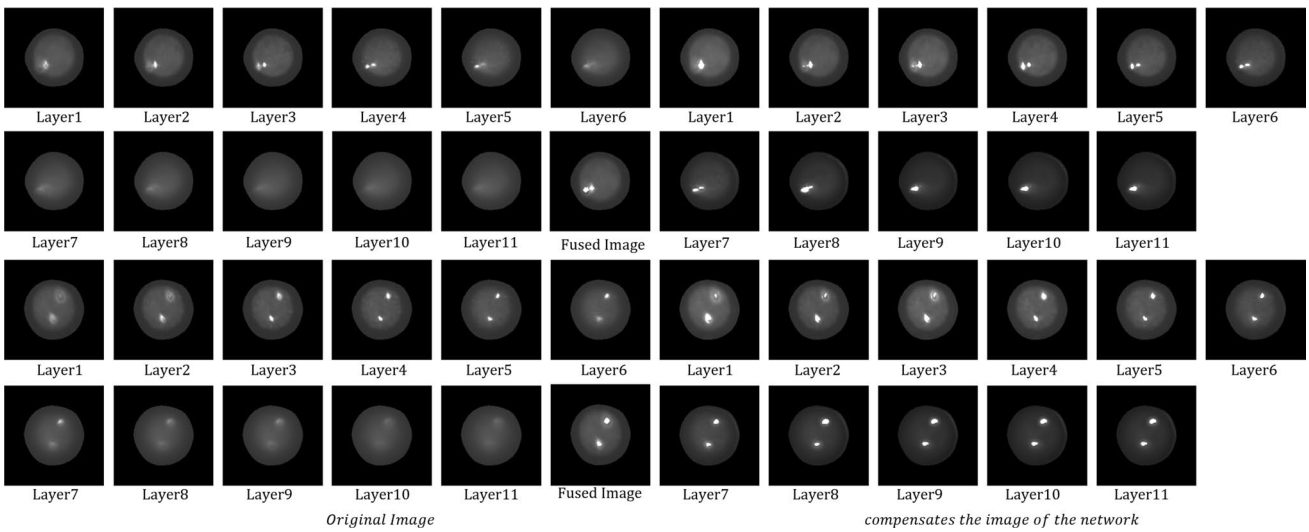

Fig. 4 Network compensation for this article

Contrast and EOG, this method is similar to Pix2Pix (p values are 0.8273 and 0.7722 respectively). However, in CII, Methods has no significant difference with other methods and performs similarly (p values are all greater than 0.05). (Detailed description is in the Supplementary Information note 6 and Fig. 7 and 8).

Unlike Cycle-GAN, which fails to significantly enhance signal intensity, GAN, which produces blurry results, and VAE, which introduces noise and artifacts, the proposed network excels in maintaining signal clarity, minimizing noise, and preserving edge and texture details. These results highlight its ability to enhance fluorescence signals effectively as shown in Fig. 4, improving the detection and distinguishability of abnormal cell characteristics while maintaining high stability and naturalness across experiments (Detailed description is in the Supplementary Information note 7 and Fig. 9).

Visualization analysis

To validate the accuracy and consistency of compensated fluorescence features, a detailed visualization analysis was conducted on the fluorescence signals of weakly expressed genes, such as RB1, DLEU, and LAMP1 genes. The process involved the following steps and findings:

Fluorescence Signal Detection: Orange Filter: Used to detect the orange fluorescence signal of the DLEU gene, marking the 13q14 region, commonly deleted in CLL and associated with prognosis. Green Filter: Observed the green fluorescence signal of the RB1 gene, marking the 13q14.2 region, where deletions may indicate complex disease progression. Blue Filter: Detected the blue fluorescence signal of the LAMP1 gene, marking the 13q34 region, which may influence prognosis.

To verify the accuracy and consistency of compensated fluorescence features, 3D reconstruction techniques were used to visualize the spatial distribution of these weakly expressed genes. Feature point detection and description algorithms were applied to extract key points, ensuring speed and accuracy in feature extraction and matching. Spatial consistency was evaluated by calculating the overlap ratio between the reconstructed image and reference image using the Dice coefficient, while reconstruction precision was assessed using the Jaccard index, quantifying the overlap area relative to the union of regions.

Visualization of Compensation Effects: Commercial tools such as Mimics and 3D Slicer were utilized to perform three-dimensional fusion reconstruction of the compensated tricolor fluorescence signal images (as shown in Fig. 5.c-l), further validating the proposed method's effectiveness. Observations across 11 layers(z-stack) of fluorescence images revealed that the compensation technique significantly enhanced fluorescence signal intensity while suppressing background interference. The reconstructed signals exhibited sharper edges, more uniform distribution, and fully preserved fluorescence signal details, as illustrated in Fig. 5.

Single-Layer Image Analysis: The probe-labeled DLEU1 gene (13q14.2 region) exhibited relatively intact orange fluorescence signals (Fig. 5a), indicating no significant deletions of this gene. The probe-labeled LAMP1 gene (13q34 region) showed blue fluorescence signals, but these were sparse, making it difficult to accurately assess fluorescence distribution (Fig. 5e). The probe-labeled RB1 gene (13q14.2 region) displayed green fluorescence signals with fragmentation or fusion phenomena, suggesting potential abnormalities and partial fluorescence feature loss (Fig. 5i). This initial analysis implies possible genomic abnormalities in the patient, with particular attention required for the RB1 gene, as its deletion may be closely associated with tumor progression. After network-based compensation, the distribution of orange fluorescence signals became clearer

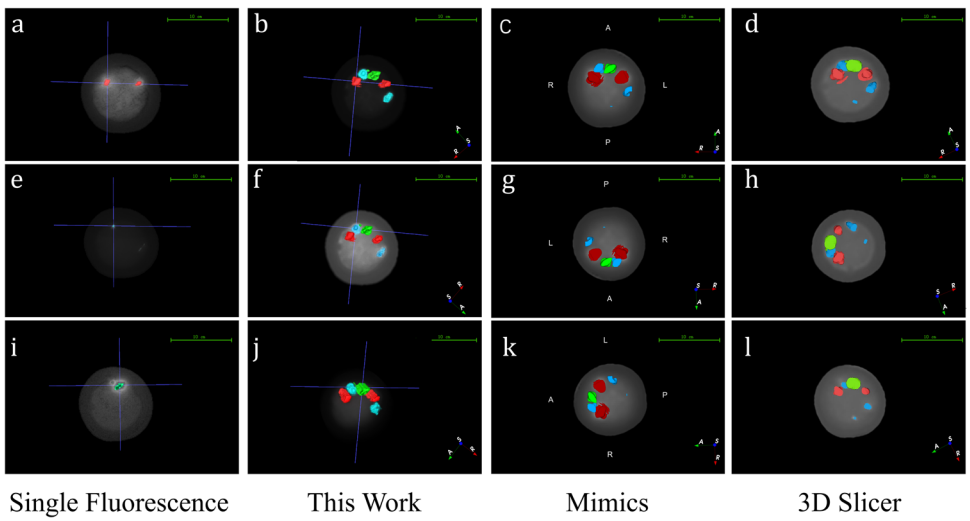

Fig. 5 Comparison of 3D Reconstruction Results

and more complete (Fig. 5b), making the signal characteristics more reliable. The blue fluorescence signals were compensated from single-fluorescence to dual-fluorescence features, enhancing the detection capability for the LAMP1 gene (Fig. 5f). Weak signal regions in the green fluorescence signals were compensated, displaying more uniform dual-fluorescence features (Fig. 5j). This improved the visibility and detection accuracy of weak fluorescence signals, addressing issues of signal blurriness caused by attenuation and background noise. Optimization of weak signal regions for genes like RB1 and LAMP1 made previously undetectable abnormal signals clearly visible, reducing the occurrence of false-negative results and improving the reliability of screening outcomes. Compensation for fragmentation and fusion phenomena in the green fluorescence signals of the RB1 gene, along with the restoration of dual-fluorescence features for the LAMP1 gene, demonstrated the method's ability to precisely identify complex chromosomal abnormalities such as deletions, breaks, and fusions.

Discussion

This study proposes a fluorescence signal enhancement and compensation framework that effectively addresses key challenges in fluorescence microscopy, especially in the diagnosis of chronic lymphocytic leukemia (CLL). By integrating automated acquisition, a hybrid global–local feature analysis, and a Cycle-GAN-based network, the framework significantly improves signal clarity, accuracy, and robustness, overcoming the limitations of traditional techniques, particularly issues such as signal attenuation, background noise interference, and image blur.

The application of this method in FISH effectively detects chromosomal abnormalities (such as RB1, DLEU1, LAMP1) and improves image quality, addressing challenges like signal fragmentation and uneven distribution. Automated acquisition greatly enhances efficiency and reproducibility, reducing human error in high-throughput genetic screening. Clinically, the framework reduces false negatives and accurately detects complex genetic abnormalities, thus supporting the implementation of personalized treatment and precision medicine.

Furthermore, the application of the framework not only limited to CLL, but also holds potential for the diagnosis of other cancers and genetic diseases. For example, by appropriately adjusting the network structure and data input, it can be used in areas such as breast cancer, lung cancer, and neurodegenerative diseases, enhancing genomic analysis, and diagnostic accuracy for these diseases. Additionally, by combining different imaging modalities, such as confocal microscopy or other molecular imaging technologies, the framework maintains high versatility, promoting its wide adoption in biomedical applications.

However, slight deviations in local features remain a challenge and require further optimization in future research to improve the framework's universality and performance across different datasets and imaging modes. Overall, this framework provides more precise and reliable technical support for the personalized diagnosis and treatment of CLL and other diseases, advancing the development of precision medicine.

Patents

The authors have filed one patent applications based on this work: fluorescence image signal data storage and color classification method (CN113539368B).

Supplementary Information The online version contains supplementary material available at https://doi.org/10.1007/s00432-025-06150-9.

Acknowledgements The authors extend their gratitude to Changchun University of Science and Technology for the provision of the necessary microscope equipment. Our thanks also go to Wuhan Baitai Gene Engineering Co., Ltd., for supplying the HER2 gene amplification detection kit and human blood cell specimen used in our FISH clinical experiments. Lastly, we wish to acknowledge the pathologists who offered their invaluable expertise and insightful evaluations throughout this study.

Author contributions Conceptualization, L.S., M.L. and X.F.; methodology, L.S. and X.F.; software, L.S. and D.S.; validation, L.S., M.L., H.Z.; formal analysis, L.S. and D.S.; investigation, L.S. and D.S.; resources, P.G. Z.W. and Z.W.; data curation, L.Z. and D.S.; writing—original draft preparation, L.S.; writing—review and editing, M.L., X.F.; visualization, L.S.; supervision, X.F.; project administration, L.S. and M.L.; funding acquisition, P.G. and Z.W. All authors have read and agreed to the published version of the manuscript.

Funding This research was funded by Jilin Provincial Scientific and Technological Development Program, grant numbers 20230401087YY, 20220201092GX.

Data availability The datasets generated during and/or analysed during the current study are available from the corresponding author on reasonable request.

Declarations

Conflict of interest The authors declare no conflicts of interest. The funders had no role in the design of the study; in the collection, analyses, or interpretation of data; in the writing of the manuscript; or in the decision to publish the results.

Ethical approval The study was conducted in accordance with the Declaration of Helsinki, and approved by the Ethics Committee of Fudan University Zhongshan Hospital (protocol code: 2022–021, date of approval: 14/02/2022).

Consent to participate Patient consent was waived due to unidentifiable information.

References

Abdelhedi F, Chalas C, Petit JM, Abid N, Mokadem E, Hizem S, Kamoun H, Keskes L, Dupont JM (2019) Altered three-dimensional organization of sperm genome in DPY19L2-deficient globozoospermic patients. J Assist Reprod Genet 36:69–77. https://doi.org/10.1007/s10815-018-1342-y

Agrawal D, Yadav AC, Tyagi PK (2024) Low-light and hazy image enhancement using retinex theory and wavelet transform fusion. Multimedia Tools Appl. https://doi.org/10.1007/s11042-024-18459-7

Bloehdorn J, Braun A, Taylor-Weiner A, Jebaraj BMC, Robrecht S, Krzykalla J, Pan H, Giza A, Akylzhanova G, Holzmann K, Scheffold A, Johnston HE, Yeh RF, Klymenko T, Tausch E, Eichhorst B, Bullinger L, Fischer K, Weisser M, Robak T, Schneider C, Gribben J, Dahal LN, Carter MJ, Elemento O, Landau DA, Neuberg DS, Cragg MS, Benner A, Hallek M, Wu CJ, Döhner H, Stilgenbauer S, Mertens D (2021) Multi-platform profiling characterizes molecular subgroups and resistance networks in chronic lymphocytic leukemia. Nat Commun 12:5395. https://doi.org/10.1038/s41467-021-25403-y

Bouilhol E, Savulescu AF, Lefevre E, Dartigues B, Brackin R, Nikolski M (2022) DeepSpot: a deep neural network for RNA spot enhancement in single-molecule fluorescence in-situ hybridization microscopy images. Biol Imaging 2:e4. https://doi.org/10.1017/s2633903x22000034

Chen Y, Lin H, Zhang W, Chen W, Zhou Z, Heidari AA, Chen H, Xu G (2024) ICycle-GAN: Improved cycle generative adversarial networks for liver medical image generation. Biomed Signal Process Control 92:106100. https://doi.org/10.1016/j.bspc.2024.106100

Eichenberger BT, Zhan Y, Rempfler M, Giorgetti L, Chao JA (2021) deepBlink: threshold-independent detection and localization of diffraction-limited spots. Nucleic Acids Res 49:7292–7297. https://doi.org/10.1093/nar/gkab546

Frankenstein Z, Uraoka N, Aypar U, Aryeequaye R, Rao M, Hameed M, Zhang Y, Yagi Y (2021) Automated 3D scoring of fluorescence in situ hybridization (FISH) using a confocal whole slide imaging scanner. Appl Microsc 51:4. https://doi.org/10.1186/s42649-021-00053-y

Goodfellow I, Pouget-Abadie J, Mirza M, Xu B, Warde-Farley D, Ozair S, Courville A, Bengio Y (2014) Generative adversarial nets. Advances in neural information processing systems 27.

Imbert A, Ouyang W, Safieddine A, Coleno E, Zimmer C, Bertrand E, Walter T, Mueller F (2022) FISH-quant v2: a scalable and modular tool for smFISH image analysis. RNA 28:786–795. https://doi.org/10.1261/rna.079073.121

Kim S, Lee J, Jeong K, Lee J, Hong T, An J (2024) Automated door placement in architectural plans through combined deep-learning networks of ResNet-50 and Pix2Pix-GAN. Expert Syst Appl 244:122932. https://doi.org/10.1016/j.eswa.2023.122932

Kloetgen A, Thandapani P, Ntziachristos P, Ghebrechristos Y, Nomikou S, Lazaris C, Chen X, Hu H, Bakogianni S, Wang J, Fu Y, Boccalatte F, Zhong H, Paietta E, Trimarchi T, Zhu Y, Van Vlierberghe P, Inghirami GG, Lionnet T, Aifantis I, Tsirigos A (2020) Three-dimensional chromatin landscapes in T cell acute lymphoblastic leukemia. Nat Genet 52:388–400. https://doi.org/10.1038/s41588-020-0602-9

Kulasinghe A, Lim Y, Kapeleris J, Warkiani M, O'Byrne K, Punyadeera C (2020) The use of three-dimensional dna fluorescent in situ hybridization (3D DNA FISH) for the detection of anaplastic lymphoma kinase (alk) in non-small cell lung cancer (NSCLC) circulating tumor cells. Cells. https://doi.org/10.3390/cells9061465

Lew M, Wilbur DC, Pantanowitz L (2021) Computational cytology: lessons learned from pap test computer-assisted screening. Acta Cytol 65:286–300. https://doi.org/10.1159/000508629

Li N, Lv T, Sun Y, Liu X, Zeng S, Lv X (2021a) High throughput slanted scanning whole slide imaging system for digital pathology. J Biophotonics 14:e202000499. https://doi.org/10.1002/jbio.202000499

Li H, Qu L, Hua Z, Wang X, Zhao W, Liu J (2021b) Fluorescence microscopy technology and applications based on deep learning. Laser Opt Prog 58:1811007

Liu Z, Gao G, Sun L, Fang Z (2021) HRDNet: High-resolution detection network for small objects. 2021 IEEE international conference on multimedia and expo (ICME).

Mabaso M A, Withey D J, Twala B (2018) Spot detection in microscopy images using convolutional neural network with sliding-window approach.

Memmel S, Sisario D, Zimmermann H, Sauer M, Sukhorukov VL, Djuzenova CS, Flentje M (2020) FocAn: automated 3D analysis of DNA repair foci in image stacks acquired by confocal fluorescence microscopy. BMC Bioinform 21:27. https://doi.org/10.1186/s12859-020-3370-8

Nelson BP, Gupta R, Dewald GW, Paternoster SF, Rosen ST, Peterson LC (2007) Chronic lymphocytic leukemia FISH panel: impact on diagnosis. Am J Clin Pathol 128:323–332. https://doi.org/10.1309/21tn2ruwkr827uw2

Osorio F, Vallejos R, Barraza W, Ojeda SM, Landi MA (2022) Statistical estimation of the structural similarity index for image quality assessment. Signal Image Video Proc. https://doi.org/10.1007/s11760-021-02051-9

Pan Z, Lau SL, Yang X, Guo N, Wang X (2023) Automatic pavement crack segmentation using a generative adversarial network (GAN)-based convolutional neural network. Results Eng 19:101267. https://doi.org/10.1016/j.rineng.2023.101267

Safaee MM, McFarlane IR, Nishitani S, Yang SJ, Sun E, Medina SM, Squire H, Landry MP (2024) Dual infrared 2-photon microscopy achieves minimal background deep tissue imaging in brain and plant tissues. Adv Funct Mater. https://doi.org/10.1002/adfm.202404709

Stachelek P, MacKenzie L, Parker D (2022) Circularly polarised luminescence laser scanning confocal microscopy to study live cell chiral molecular interactions. Nat Commun 13:553. https://doi.org/10.1038/s41467-022-28220-z

Suradi SH, Abdullah KA (2021) Digital mammograms with image enhancement techniques for breast cancer detection: a systematic review. Curr Med Imaging 17:1078–1084. https://doi.org/10.2174/1573405617666210127101101

Tian Z, Qu P, Li J, Sun Y, Li G, Liang Z, Zhang W (2023) A survey of deep learning-based low-light image enhancement. Sensors (Basel). https://doi.org/10.3390/s23187763

Trieu T, Oluwadare O, Cheng J (2019) Hierarchical reconstruction of high-resolution 3D models of large chromosomes. Sci Rep 9:4971. https://doi.org/10.1038/s41598-019-41369-w

Wang X, Chen X, Li Y, Liu H, Li S, Zhang RR, Zheng B (2012) Fluorescence in situ hybridization (FISH) signal analysis using automated generated projection images. Anal Cell Pathol (Amst) 35:395–405. https://doi.org/10.3233/acp-2012-0068

Wang K, Zheng M, Wei H, Qi G, Li Y (2020) Multi-modality medical image fusion using convolutional neural network and contrast pyramid. Sensors (Basel). https://doi.org/10.3390/s20082169

Wang C, Li Y, Huang K, Yang C, Gui W (2022) VAE4RSS: A VAE-based neural network approach for robust soft sensor with application to zinc roasting process. Eng Appl Artif Intell 114:105180. https://doi.org/10.1016/j.engappai.2022.105180

Wang SZ, Jiang F, Zhu DL, Yang TL, Guo Y (2023a) Application of Hi-C technology in three-dimensional genomics research and disease pathogenesis analysis. Yi Chuan 45:279–294. https://doi.org/10.16288/j.yczz.22-390

Wang X, Yao T, Liu M, Zheng K, Zhao C, Xiao L, Zhu D (2023b) A normalized absolute values adaptive evaluation function of image clarity. Sensors (Basel). https://doi.org/10.3390/s23229017

Yadav AC, Kolekar MH, Zope MK (2025) Modified recurrent residual attention U-Net model for MRI-based brain tumor segmentation. Biomed Signal Process Control 102:107220. https://doi.org/10.1016/j.bspc.2024.107220

Yang L, Hou H, Li J (2025) Frontiers in fluorescence imaging: tools for the in situ sensing of disease biomarkers. J Mater Chem B 13:1133–1158. https://doi.org/10.1039/d4tb01867b

Zhang W, Jin S, Zhuang P, Liang Z, Li C (2023) Underwater image enhancement via piecewise color correction and dual prior optimized contrast enhancement. IEEE Signal Process Lett 30:229–233. https://doi.org/10.1109/LSP.2023.3255005

Zhu J-Y, Park T, Isola P, Efros A A (2017) Unpaired image-to-image translation using cycle-consistent adversarial networks. Proceedings of the IEEE international conference on computer vision.